Polarizational nonlinear optical response of photonic structures with a liquid crystal defect

Etienne Brasselet,[1,*] Andrey E. Miroshnichenko,[2] Deng Feng Chen,[2]
Wieslaw Krolikowski,[2] and Yuri S. Kivshar[2]

[1]*Centre de Physique Optique Moléculaire et Hertzienne, Université Bordeaux 1, CNRS, 351 Cours de la Libration,
33405 Talence Cedex, France*
[2]*Nonlinear Physics Centre and Laser Physics Centre, Centre for Ultra-high bandwidth Devices for Optical Systems
(CUDOS), Research School of Physics and Engineering, Australian National University,
Canberra ACT 0200, Australia*
Corresponding author: e.brasselet@cpmoh.u-bordeaux1.fr

We demonstrate experimentally that a one-dimensional photonic crystal with a homeotropic nematic liquid crystal defect behaves as a polarization-sensitive nonlinear all-optical device. We study statics and dynamics of the nonlinear optical response for linearly and circularly polarized beams and show enhanced light sensitivity and polarization self-modulation effects. © 2009 Optical Society of America
OCIS codes: 190.0190, 230.1150, 230.3720, 230.4320.

Since the introduction of the photonic crystals concept, considerable advances have been achieved in tailoring material architectures toward a versatile structural control of light propagation [1]. The optical properties of photonic crystals can be tuned by external fields that offer flexible technical opportunities when designing reconfigurable optical devices. Among available strategies, liquid crystals (LCs) are recognized as unique materials that combine birefringence and periodic spatial ordering with a pronounced sensitivity to external fields [2,3]. Thermal and electrical tuning have been achieved for photonic structures infiltrated by LCs [4–6]. The manipulation of light by light in photonic LC fibers [7], one-dimensional natural cholesteric LC photonic structures [8], or planar photonic crystals [9] is based on resonant LCs mixtures, where the LC order parameter is optically controlled through the thermal or isothermal phase transition. However, only a few studies on LC infiltrated photonic structures are devoted to the nonresonant case based on orientational nonlinearities of nematic LCs (NLCs), including the studies of periodic structures with an NLC defect [10–12].

Here we demonstrate that a one-dimensional photonic crystal with an NLC defect behaves as a polarization-sensitive nonlinear all-optical device. We perform the passive and active optical characterization for linearly and circularly polarized light. Defect modes are shown to significantly increase the NLC optical sensitivity. In the circular polarization case, self-sustained polarization dynamics is observed, which can be easily converted into amplitude self-modulation using polarizing optics.

Experiments are performed using an NLC (E7) microwedge sandwiched in between two identical dielectric periodic structures made of seven alternating layers of SiO_2 and TiO_2 with thicknesses of $\simeq 91$ and $\simeq 55$ nm, respectively. The microwedge has an averaged thickness of $\langle L \rangle = 23$ μm and an apex angle of $\alpha \sim 0.6$ mrad, as illustrated in Fig. 1. The inner sur-

faces of the two dielectric stacks are chemically treated by surfactant cetyl trimethyl ammonium bromide to ensure a strong homeotropic alignment. Hence, the local averaged molecular orientation represented by a unit vector **n**, called the director, is uniformly parallel to the z axis at rest (Fig. 1). The setup consists of a cw laser, operating at wavelength of $\lambda = 532$ nm, that is focused at normal incidence on the sample using a 10 cm focal length lens (Fig. 1). The beam spot at the sample location has a Gaussian profile with a $w_0 = 11$ μm waist at $\exp(-2)$ of its maximum intensity. A half-wave plate and a polarizer control the input beam power whose polarization is adjusted by a quarter-wave plate. The output light is collected by a second lens and the intensities of its (x,y) or left- or right-handed circularly polarized electric field components, $I_{x,y}$ and $I_{\sigma\pm}$, are monitored using a quarter-wave plate placed in front of a Wollaston prism and two photodiodes (Fig. 1).

The use of a microwedged NLC defect layer allows the spectral characterization and adjustment of the photonic structure at a fixed wavelength. Indeed, the optical defect modes frequencies arising from the periodicity breaking depend on the optical path of the NLC wedge, $2\pi n_\perp L(x)/\lambda$, where $n_\perp$ is the refractive index perpendicular to **n** and $L(x)$ is the local wedge thickness. From an experimental point of view the lateral displacement of the whole structure along the x axis (Fig. 1) enables one to obtain an equivalent
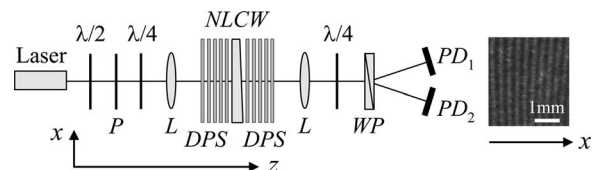
Fig. 1. Experimental setup. $\lambda/2$ and $\lambda/4$, half- and quarter-wave plates; P, polarizer; L, lens; DPS, dielectric periodic structure; NLCW, NLC microwedge; WP, Wollaston prism; $PD_{1,2}$, photodiodes. Right: transmission fringes pattern when the structure is illuminated with a spatially extended laser beam.

transmission spectrum, in the limit of $\alpha \ll 1$, as shown in Fig. 2(a) where the beam power is sufficiently low to prevent any light-induced effects. In Fig. 2(a), the solid curve is a multi-Lorentzian fit, and the fine structure of a single peak is given in Fig. 2(c). Numerically the problem is conveniently solved in the plane-wave approximation (z spatial dependence only) [11] by using the Berreman 4×4 matrix approach [13]. By taking an ideal parallel NLC slab of variable thickness L around $\langle L_0 \rangle$, which is the nearest value to $\langle L \rangle$ that matches a defect mode frequency, we obtain the transmission spectra shown in Fig. 2(b).

We measure a free spectral range $\Delta x = 290 \pm 1$ μm, which gives an estimate for the apex angle $\alpha = \lambda/(2n_\perp \Delta x)$. Taking the typical value $n_\perp = 1.52$ we obtain $\alpha \simeq 0.6$ mrad. Clearly, two distinct differences emerge when comparing observations to simulations. Namely, (i) the maximal transmission, T_{max}, associated with the defect mode resonances and (ii) the transmission peaks FWHM, δx. First, $T_{max,exp} = 0.18 \pm 0.03$ [Fig. 2(a)] whereas the predicted value is $T_{max} = 1$ [Fig. 2(b)]. Second, $\delta x_{exp} = 26.8 \pm 1.6$ μm [Fig. 2(c), solid curve] whereas we calculate $\delta x = 4.8$ μm [Fig. 2(c), dashed curve]. Such discrepancies can be explained noting that the lateral displacement of the beam during multiple reflections reduces the visibility of the interference process, which leads to a lower T_{max} and a larger δx as much as the ratio $w_0/\Delta x$ is large.

The detuning parameter, originally defined in the spectral domain as $\lambda - \lambda_d$ where λ_d is the nearest defect mode frequency from the laser wavelength [11], is controlled here via lateral positioning of the structure. This allows us to evidence the drastic power reduction for activating the NLC by light through the optical Fréedericksz transition [11]. For this purpose we set the detuning parameter to zero and monitor the transmitted power, P_{output}, as a function of the incident power, P_{input}. The results are shown in Fig. 3 for a linearly polarized beam. At low power we observe a linear dependence whose slope defines the maximal transmission for the selected defect mode. Above threshold power $P_{th} = 9.7 \pm 0.3$ mW (Fig. 3), the behavior still exhibits linear features but with a
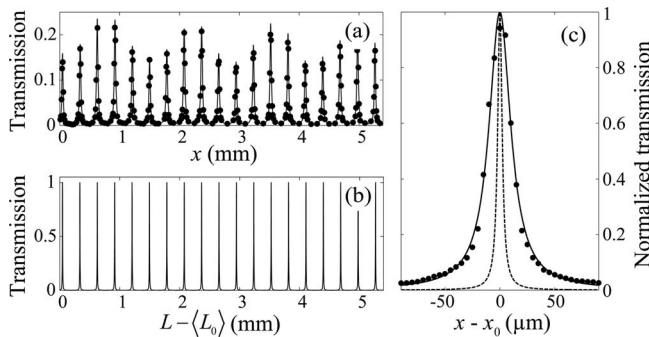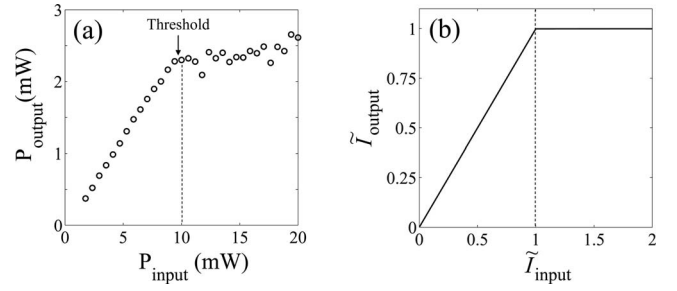
Fig. 3. Output versus input power. (a) Experiment. The dashed line indicates the reorientation threshold of the LC defect layer. (b) Numerical results. $\tilde{I}$ is the intensity normalized to the reorientation threshold intensity.

much less steep slope. Such a transmission decrease for $P > P_{th}$ indicates effective refractive index changes of the NLC layer, i.e., all-optical reorientation. This threshold should be compared to the one obtained using a single homeotropic NLC parallel slab with thickness $L = \langle L \rangle$ and identical beam waist. By looking at the transverse intensity profile of the output beam, which is altered by self-focusing effects above threshold, as a function of the input power we measure $P_{th,slab} = 100 \pm 5$ mW. Hence a typical power threshold reduction factor $f_{exp} \sim 10$ is reached, whereas we calculate $f = 25$. The discrepancy again comes from the less light confinement at the defect modes owing to the microwedge structure. Above threshold, the output power P_{output} is almost constant independently of the input power P_{input} [Fig. 3(a)], indicating that any increase of the latter is almost compensated by a drop in the transmission due to the defect mode frequencies redshift associated with a LC reorientation amplitude increase [11]. In fact, this two-slope behavior agrees with simulations [Fig. 3(b)] and confirms another theoretical result of [11] under linear polarization, namely, sharp change of the transmission during reorientation, which is intimately related to the presence of the periodic structure.

For the linear polarization case, the above threshold orientational states are static, and output polarization is unchanged with respect to the input one, whereas we find a more complicated picture when the incident polarization is circular. In practice, the third normalized Stokes parameter s_3 of the incoming beam is set to $|s_3| > 0.99$, an ideal circular polarization being defined by $|s_3| = 1$. Above the threshold, we observe temporal oscillations of $I_{x,y}(t)$. This is demonstrated in Fig. 4(a), where the signal $I_x(t)$ exhibits a periodic behavior just above the reorientation threshold when the detuning parameter is set to zero, as confirmed by the fast Fourier transform shown in Fig. 4(b). In addition, $I_{\sigma\pm}$ are found to be constant [inset of Fig. 4(a)]; so is the total output power. Thus, the effective refractive index of the NLC defect layer is time independent. By introducing the polar (Θ) and azimuthal (Φ) angles to define the director, $\mathbf{n} = (\sin\Theta\cos\Phi, \sin\Theta\sin\Phi, \cos\Theta)$, this case is characterized as $\partial_t\Theta = 0$ and $\partial_z\Theta \neq 0$. Since it is known [14] that (i) ordinary and extraordinary waves are coupled inside a twisted ($\partial_z\Phi \neq 0$) and reoriented

Fig. 2. Transmission versus beam waist lateral x position. (a) Experimental data (symbols) and multi-Lorentzian fit (solid curve). (b) Numerical result. (c) Single normalized transmission peak located at $x = x_0$, the dashed curve being the numerical result.
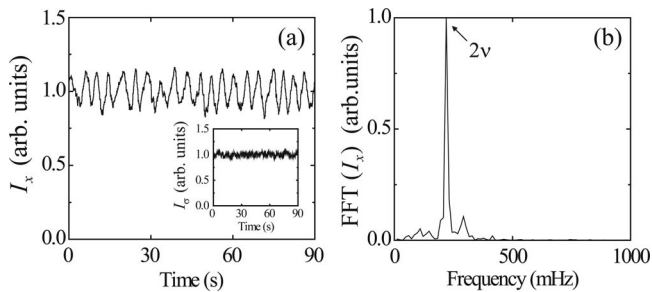
Fig. 4. (a) Intensity of x polarized component of output light versus time under circular incident polarization. Inset: one of the two circularly polarized components. (b) Fast Fourier transform of $I_x(t)$.

($\partial_z\Theta \neq 0$) NLC and (ii) polar optical torque directly depends on extraordinary wave intensity, we conclude that the twisted distortions are also time independent, $\partial_{tz}\Phi = 0$ (if not, $\partial_t\Theta \neq 0$).

The observed polarization dynamics thus results from the regular rotation of the output polarization ellipse in the (x,y) plane. In fact, this is the signature of the director precession around the z axis, at constant frequency ν, as a consequence of continuous light spin angular-momentum transfer to the birefringent NLC [15]. In that case, one has $\partial_t\Phi = 2\pi\nu$ where the molecular rotation frequency ν is half the frequency of $I_x(t)$ owing to the π-rotation invariance of the polarization ellipse.

An estimate of the rotation frequency is grasped from the single-slab case. Indeed, at the reorientation threshold we get, in the limit $\lambda \ll L$, the analytical expression $\nu_{\text{slab}} \simeq \widetilde{\rho}(1 - \cos\Delta)/(2\pi\tau\Delta)$ [16], where $\Delta \simeq \pi$ is the total light-induced phase delay; τ is a characteristic orientational relaxation time, with $\tau \simeq 0.5$ s for $L = 23$ μm; and $\widetilde{\rho} = [1 + \sqrt{2}L/(\pi w_0)]^2$ is a correcting factor accounting for finite beam size effects [17], with $\widetilde{\rho} \simeq 3.8$. We get $\nu_{\text{slab}} \simeq 720$ mHz, which is a few times higher than the observed value $\nu = 110$ mHz [Fig. 4(b)]. Observations thus indicate that the light–matter spin angular momentum transfer processes strongly depend on the presence of the periodic structure. The theoretical description of such processes is under current investigation.

The application potential of such structures is demonstrated here in terms of polarization dynamics, which can be further converted into amplitude modulation by using polarizing optics [Fig. 4(a)]. However, pure amplitude self-modulation is expected, too, in the presence of nutation regimes ($\partial_t\Theta \neq 0$) that are already known to appear in the single-slab geometry [18].

In conclusion, we have experimentally demonstrated all-optical switching of a one-dimensional dielectric periodic structure with a homeotropic NLC defect, including the drastic reduction of the optical reorientation threshold and a self-sustained oscillatory dynamics for circularly polarized light associated with a rotation of the director. These results suggest an alternative approach toward all-optical LC infiltrated photonic structures that exhibit both phase and amplitude self-modulation of the transmitted light.

References

1. J. D. Joannopoulos, R. D. Meade, and J. N. Winn, *Photonic Crystals: Molding the Flow of Light*, 2nd ed. (Princeton U. Press, 2008).
2. K. Busch and S. John, Phys. Rev. Lett. **83**, 967 (1999).
3. K. Yoshino, Y. Shimoda, Y. Kawagishi, K. Nakayama, and M. Ozaki, Appl. Phys. Lett. **75**, 932 (1999).
4. Y.-K. Ha, Y.-C. Yang, J.-E. Kim, H. Y. Parka, C.-S. Kee, H. Lim, and J.-C. Lee, Appl. Phys. Lett. **79**, 15 (2001).
5. S. W. Leonard, J. P. Mondia, H. M. Van Driel, O. Toader, S. John, K. Busch, A. Birner, U. Gösele, and V. Lehmann, Phys. Rev. B **61**, R2389 (2000).
6. D. Kang, J. E. Maclennan, N. A. Clark, A. A. Zakhidov, and R. H. Baughman, Phys. Rev. Lett. **86**, 4052 (2001).
7. T. T. Alkeskojld, L. A. Bjarklev, D. S. Hermann, Anawati, J. Broeng, J. Li, and S. T. Wu, Opt. Express **12**, 5857 (2004).
8. H. Yoshida, C. H. Lee, Y. Miura, A. Fujii, and M. Ozaki, Appl. Phys. Lett. **90**, 071107 (2007).
9. B. Maune, J. Witzens, T. Baehr-Jones, M. Kolodrubetz, H. Atwater, A. Scherer, R. Hagen, and Y. Qiu, Opt. Express **13**, 4699 (2005).
10. A. E. Miroshnichenko, I. Pinkevych, and Y. S. Kivshar, Opt. Express **14**, 2839 (2006).
11. A. E. Miroshnichenko, E. Brasselet, and Y. S. Kivshar, Appl. Phys. Lett. **92**, 253306 (2008).
12. U. A. Laudyn, A. E. Miroshnichenko, W. Krolikowski, D. F. Chen, Y. S. Kivshar, and M. A. Karpierz, Appl. Phys. Lett. **92**, 203304 (2008).
13. D. W. Berreman, J. Opt. Soc. Am. **62**, 502 (1972).
14. E. Brasselet, T. V. Galstian, L. J. Dubé, D. O. Krimer, and L. Kramer, J. Opt. Soc. Am. B **22**, 1671 (2005).
15. E. Santamato, B. Daino, M. Romagnoli, M. Settembre, and Y. R. Shen, Phys. Rev. Lett. **57**, 2423 (1986).
16. L. Marrucci, G. Abbate, S. Ferraiuolo, P. Maddalena, and E. Santamato, Phys. Rev. A **46**, 4859 (1992).
17. E. Brasselet, A. Lherbier, and L. J. Dubé, J. Opt. Soc. Am. B **23**, 36 (2006).
18. E. Brasselet and L. J. Dubé, Phys. Rev. E **73**, 021704 (2006).